Contents lists available at ScienceDirect

Applied Surface Science

journal homepage: www.elsevier.com

Full Length Article

Photocatalytic decomposition of methanol-water solution over N-La/TiO_2 photocatalysts

Lada Dubnová[a], Magdalena Zvolská[a], Miroslava Edelmannová[b], Lenka Matějová[b], Martin Reli[b], Helena Drobná[a], Piotr Kuśtrowski[c], Kamila Kočí[b], Libor Čapek[a,*]

[a] Faculty of Chemical Technology, University of Pardubice, Studentská 573, Pardubice, Czech Republic
[b] Institute of Environmental Technology, VŠB-Technical University of Ostrava, 17.listopadu 15/2172, Ostrava – Poruba, Czech Republic
[c] Faculty of Chemistry, Jagiellonian University, Gronostajowa 2, 30-387 Kraków, Poland

ARTICLE INFO

Keywords:
Hydrogen production
N-La/TiO_2
Surface oxygen species
Oxygen vacancies

ABSTRACT

Manuscript focuses on the role of N-doping on photocatalytic behaviour of N-La/TiO_2 materials in decomposition of methanol-water solution. N-La/TiO_2 materials were prepared with approximately the same amounts of La (0.14–0.16 wt%) and different amounts of N (0.33–0.97 at. % of surface nitrogen). Addition of small amount of surface nitrogen significantly increased the amount of hydrogen produced for N-La/TiO_2 photocatalysts in contrast to TiO_2 and La/TiO_2. The chemical composition (XRF, AAS, XPS), structural (XRD, Raman, XPS, TEM), textural (N_2-adsorption) and optical properties (DRS) were studied. N-La/TiO_2 materials showed approximately the same specific surface area and crystallite size, with values ranging for La/TiO_2 and N/TiO_2 photocatalysts. For studied N-La/TiO_2 photocatalysts, the photocatalytic activity increased with the increasing amount of surface nitrogen (interstitial positions, XPS), and subsequently with increasing amount of oxygen vacancies (Raman spectroscopy) and decreasing amount of surface oxygen species (surface lattice O species and hydroxyl groups, XPS).

1. Introduction

Photocatalytic hydrogen production is an attractive topic [1]. Great attention is focusing on the formation of hydrogen by photocatalytic water splitting processes [2]. Higher amounts of hydrogen were then published after the addition of alcohol, i.e. in a water-alcohol solution (mainly methanol); e.g. by using of Cu/TiO_2 [3], Cu-In_2O_3-TiO_2 [4], Pt/Cr(Fe)-$La_2Ti_2O_7$ [5], Pt/TiO_2 [6], Ag/TiO_2 [7], Bi_2S_3/TiO_2 [8], LaOF [9] and Au/TiO_2 [10,11] photocatalysts. Methanol has lower splitting energy than water and it is added to the reaction as a sacrificial agent [10]. The mechanism of the photocatalytic decomposition of methanol-water solution has been studied by many authors in detail [1,10,12]. The reaction can go through the direct oxidation of methanol using holes and the indirect oxidation of methanol using hydroxyl radical.

TiO_2 is one of the most studied photocatalysts [4,13–15]. The crystallite structure of anatase can contain different types of defects, with the most important ones being those creating unpaired electrons or oxygen vacancies [16]. Both types of defects act as the charge traps and affect the rate of the recombination of hole-electron pairs [17]. The oxygen vacancies can be described as unsaturated local structure in the vicinity of Ti^{3+} or other metal ions that substitute Ti^{4+} ions of anatase lattice [18]. The positive influence of oxygen vacancies on the photocatalytic behaviour of TiO_2 is generously accepted [16]. EPR spectroscopy is able to analyse oxygen vacancies due to the detection of the inner paramagnetic centres (Ti^{3+}) [19]. Raman spectroscopy uses a shift in the maximum of the most intensive band characteristic to the anatase, but unfortunately the position of this band is affected not only by the amount of defects, but also by the crystallite size of TiO_2 [20]. One of the main disadvantages of TiO_2 is its low efficiency due to a rapid recombination of electrons and holes. However, this rate may be reduced by addition of metals promoting the separation of electrons and holes and reducing the rate of recombination [21]. Lanthanum can improve the properties of semiconductor materials due to its [Xe] $5d^16s^2$ [22] configuration. Lanthanum ions are unable to enter into titanium dioxide lattice due to its large ionic radius (1.170 Å) com-

* Corresponding author.
Email address: libor.capek@upce.cz (L. Čapek)

https://doi.org/10.1016/j.apsusc.2018.11.098
Received 20 August 2018; Received in revised form 2 November 2018; Accepted 11 November 2018
Available online xxx

pared to titanium ions (0.745 Å) [23,24]. Lanthanum can be located on surface lattices resulting in a higher density of surface oxygen vacancies [25,26] and be dispersed in the form of La_2O_3 on the surface of TiO_2 resulting in a lower density of oxygen vacancies. Titanium ions can also replace the lanthanum ions in its oxide form resulting in a charge imbalance. This imbalance can be offset by the adsorption of hydroxide ions on the surface that can react with holes forming hydroxyl radicals that oxidize surface adsorbed substances and suppress recombination of electrons and holes. However, this mechanism describes the situation only at low concentration of metals, because at its high concentrations the density of the space charge is reduced, thus facilitating the recombination [27]. The doping of TiO_2 with lanthanum may also reduce the particle size, increase the specific surface area and increase the thermal stability of the materials [28,29].

Nitrogen represents one of the very attractive and highly studied non-metal dopant (e.g. [30,31]). Addition of nitrogen into TiO_2 leads to the nitrogen in substitutional and interstitial positions [32–34]. Substitutional position of nitrogen means the direct replacement of oxygen in the lattice. Interstitial position of nitrogen means the formation of Ti-O-N, where nitrogen is incorporated into interstitial sites within the crystal lattice. Zhang et al. [35] also reported that nitrogen can exist as a surface species. Addition of N into TiO_2 narrows band gap energy [34,36–38] and improves the photocatalytic activity of N-based materials under visible light. Nitrogen loading into TiO_2 photocatalyst also increases the amount oxygen vacancies [32,34].

N-La/TiO_2 photocatalysts have been studied in degradation of methyl orange [37,39], naphthalene [40] and Rhodamine B [31,41,42], and in propylene oxidation [43]. Improving the activity of the N-La/TiO_2 photocatalysts has been explained:

- by the narrowing of the band gap ($La_2Ti_2O_7$ nanosheets) [37],
- by synergistic effect including inhibition of recombination of photogenerated electrons and holes, shift of band gap energy to lower values, an increase in amount of surface hydroxyls and an increase in the specific surface area and volume of pores [40],
- due to the unique 3D hierarchical porous nanostructures with the high specific surface area [39],
- due to high specific surface area and a shift of band gap energy to lower values [43],
- by hindering the recombination of electron-hole pairs (La-effect) and narrowing of the band gap energy (N-effect) [31,41,42,44].

The synergetic effect mentioned above have also been reported for other materials, e.g. AuN-TiO_2 [45], AgN-TiO_2 [46].

This manuscript focuses on the combined TiO_2 doping by low concentration of lanthanum (chosen based on our previous work [12]) and nitrogen that can lead to the synergistic effect of the above-mentioned properties. The TMEDA (N,N,N′,N′-tetramethylethane-1,2-diamine) has been used as a nitrogen precursor. TMEDA is a fine nitrating agent using a chelate effect to form stronger bonds to Ti and is suitable for materials with low nitrogen concentrations [38]. The materials were prepared with approximately the same amount of La and changing amount of nitrogen in order to stress the role of N doping on the properties and photocatalytic behaviour of N-LaTiO_2 photocatalysts.

2. Experimental

2.1. Preparation of materials

TiO_2, N-La/TiO_2, N/TiO_2 and La-TiO_2 were prepared by the sol-gel method in a reverse micellar medium. TiO_2 and La-TiO_2 materials were discussed in more detail in Ref. [12]. The materials were denoted as X at. % N/TiO_2 and X at. % N-La/TiO_2, where X is the surface concentration of nitrogen determined by XPS technique. In the first step, 0.0187 g of $La(NO_3)_3{\cdot}6H_2O$ (99.9%, Sigma-Aldrich) was dissolved in 1.04 ml absolute ethanol (water content < 0.2%, Penta Ltd.). Meanwhile, 26.4 ml cyclohexane (≥99.9%, Sigma-Aldrich) was mixed with 11.7 ml Triton 114 (laboratory grade, Sigma-Aldrich) and 0.79 ml deionized water. Both solutions were mixed for 15 min and then stirred together for 15 min. In particular, 13 ml of titanium (IV) isopropoxide (99.999%, Sigma-Aldrich) was mixed with appropriate amount of TMEDA (99%, Sigma-Aldrich) and poured into the previous solution. The amount of TMEDA was 13.17 ml (0.46 at. % N/TiO_2), 1.89 ml (0.97 at. % N-La/TiO_2), 9.40 ml (0.36 at. % N-La/TiO_2) and 13.17 ml (0.33 at. % N-La/TiO_2). The surface concentration of nitrogen is oppositely to the amount of TMEDA that is explained below. The final solution was stirred for 10 min and then poured into Petri dishes to a height of about 1–2 mm for 24 h. After gelation, the material was calcined in a muffle furnace at 450 °C with step 5 °C/min for 4 h.

2.2. Characterization of materials

X-ray fluorescence (XRF) was measured on a wave-dispersion X-ray fluorescence spectrometer (Spektroskop MAKC-GV, Spectron NPO Ltd., Russia) with a top vacuum. Atomic absorption spectroscopy was measured on an Elementar vario EL III instrument (Elementar, Germany).

X-ray diffraction (XRD) was measured in the reflection mode with Bragg-Brentano geometry using Rigaku SmartLab diffractometer (Rigaku, Japan) equipped with a D/teX Ultra detector [47]. Crystallite size, lattice parameters and phase composition were determined by the PDXL 2 software (Rigaku, Japan) with the ICDD-PDF-2 spectra library. Raman spectra were measured on a Nicolet DXR SmartRaman spectrometer (Thermo Fisher Scientific, USA) [47]. Specific surface area was measure on an automated 3Flex volumetric instrument (Micromeritics Instruments, USA) [47]. The value of specific surface area (S_{BET}) was calculated by using the BET theory. Diffuse reflectance spectra were measured in quartz cuvettes using a GBS CINTRA 303 spectrometer (GBC Scientific Equipment, Australia) equipped with an integrating sphere [47]. Kubelka–Munk function was calculated based on the equation $F(R_\infty) = (1-R_\infty)^2/(2{\cdot}R_\infty)$, where R_∞ is the diffuse reflectance from a semi-infinite layer. Indirect band gap energy was determined from the dependence of $(\alpha{\cdot}h{\cdot}\nu)^{1/2}$ against photon energy, where it is possible to assume that absorption coefficient (α) is approximately equal to the Kubelka–Munk function.

X-ray photoelectron spectra (XPS) were recorded by Prevac photoelectron spectrometer with X-ray radiation source Al Kα (E = 1486.6 eV) at a constant pass energy of 100 eV for survey and high resolution modes. Binding energies of Ti 2p, O 1s, La 3d, La 4d, C 1s and N 1s photoelectron peaks were referenced to the C 1s core level (E_b = 285.0 eV) [47].

The morphology of particles was investigated on a transmission electron microscope (TEM) JEOL 2010 HC (JEOL Ltd., Japan). The average size of the nanoparticles was obtained by measuring of 100 nanoparticles.

2.3. Photocatalytic test

The photocatalytic decomposition of methanol was carried out in homemade stainless-steel batch photoreactor with 8 W mercury lamp (λ = 365 nm). The photocatalytic procedure was described in detail recently [47].

3. Results and discussions

3.1. Structural and optical properties of La/, N/ and N-La/TiO_2

Table 1 gives the concentration of La in the studied materials determined by XRF. La/TiO_2 contained the real amount of La 0.18 wt%

Table 1
Chemical (XRF), textural and optical properties of studied photocatalysts.

Sample	Content of La (%)	S_{BET} (m^2/g)	Indirect band gap (eV)
TiO_2	–	73	2.97
La/TiO_2	0.18	73	2.96
0.33 at. % N-La/TiO_2	0.16	63	2.99
0.36 at. % N-La/TiO_2	0.16	67	2.98
0.97 at. % N-La/TiO_2	0.14	62	2.98
0.46 at. % N/TiO_2	–	39	2.93

that is close to the theoretical amount of La 0.20 wt%. N-La/TiO_2 photocatalysts were prepared to give the same La/Ti molar ratio as in the case of La/TiO_2. This way was chosen, as it is hard to predict the amount of nitrogen loading and the residual amount of TMEDA precursor during the preparation of N-La/TiO_2 photocatalysts. Therefore, the real amount of La in N-La/TiO_2 photocatalysts was slightly lower, i.e. in the range of 0.16 and 0.14 wt% La. The nitrogen and carbon content was determined by atomic absorption spectroscopy, none of the studied materials exhibited the presence of nitrogen and carbon above the detection limit of the instrument, i.e. above 0.1 wt% N or C.

Fig. 1 shows the X-ray patterns of TiO_2, La/, N/ and N-La/TiO_2 photocatalysts. All materials exhibited diffraction lines at $2\theta \approx 29.4°$, 43.1°, 44.4°, 45.2°, 56.3°, 63.6°, 64.8°, 74.2°, 82.0° and 83.9° reflecting (1 0 1), (1 0 3), (0 0 4), (1 1 2), (2 0 0), (1 0 5), (2 1 1), (2 0 4), (1 1 6) and (2 2 0) planes of the anatase phase (ICDD PDF, 00-021-1272). In addition, diffraction pattern of N/TiO_2 exhibited diffraction line at $2\theta \approx 31.9°$ corresponding to the reflection plane (1 1 0) of the rutile phase (ICDD PDF, 01-071-0650). No further diffraction lines were observed in the diffraction patterns. Thus, while TiO_2, La/TiO_2 and N-La/TiO_2 materials contained pure anatase phase, N/TiO_2 contained the mixture of anatase and rutile phases. Lanthanum is known as the stabilizer of the anatase phase before its transformation into rutile, at a low concentration of La [22,48]. Thus, though rutile phase was observed in N/TiO_2, the presence of La stabilized the formation of pure anatase phase in N-La/TiO_2 materials.

Table 2 gives the crystallite sizes and the lattice parameters of TiO_2. While La/TiO_2 exhibited only slightly higher crystallite size than pure TiO_2, the crystallite size of N/TiO_2 was significantly higher than pure TiO_2. The crystallite sizes of N-La/TiO_2 were in the range of

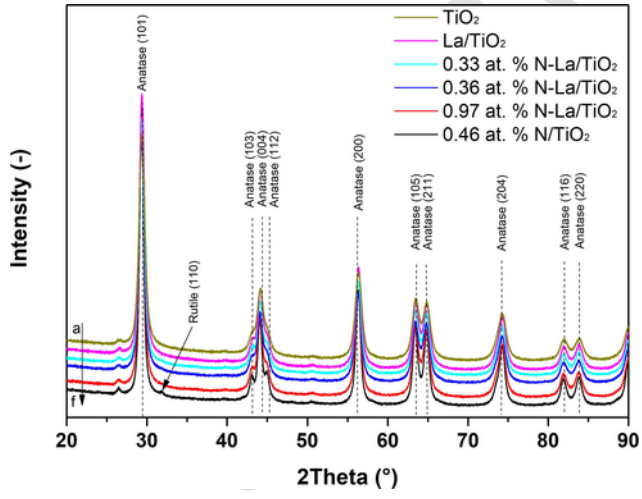

Fig. 1. Diffraction patterns of (a) TiO_2, (b) La/TiO_2, (c) 0.33 at. % N-La/TiO_2, (d) 0.36 at. % N-La/TiO_2, (e) 0.97 at. % N-La/TiO_2, (f) N/TiO_2.

Table 2
Crystallite size and lattice parameters of photocatalysts from XRD measurement, the average size of nanoparticles based on TEM.

Sample	D(Å) TEM	D(Å) XRD	Lattice parameters		
			a (Å)	c (Å)	V_{cell} (Å^3)
TiO_2	111	96	3.7874	9.5112	136.43
La/TiO_2	121	104	3.7909	9.5179	136.78
0.33 at. % N-La/TiO_2	–	139	3.7897	9.5137	136.64
0.36 at. % N-La/TiO_2	–	127	3.7893	9.5097	136.54
0.97 at. % N-La/TiO_2	135	141	3.7899	9.5151	136.67
0.46 at. % N/TiO_2	146	181	3.7844	9.5082	136.72

127–141 Å, i.e. between the values for La/TiO_2 and N/TiO_2. The lattice parameters of the individual photocatalysts were almost not changed. It corresponds to the fact that lanthanum was not incorporated into the TiO_2 lattice that could be expected from the different atomic radius of lanthanum (1.170 Å) and titanium ions (0.745) [23,24].

Fig. 2 shows the TEM images. All materials represented good uniformity of particles, similar in size and shape. Table 2 gives the average size of the nanoparticles of TiO_2, La/TiO_2, N/TiO_2 and 0.96 at. % N-La/TiO_2. All values are close to that determined by XRD. It also should be mentioned that EDS mapping reflected the presence of Ti, O and C, but the presence of N and La was below the detection limit.

Table 1 gives the specific surface area of studied materials. The highest specific surface area of 73 m^2/g exhibited TiO_2 and La/TiO_2. On the other hand, N/TiO_2 exhibited the smallest specific surface area of 39 m^2/g. N-La/TiO_2 materials possessed approximately the same specific surface area in the range of 62–67 m^2/g, i.e. between the values for La/TiO_2 and N/TiO_2 photocatalysts. So, the materials with the smallest specific surface area exhibited the highest particle size and vice versa. While the addition of low amount of La itself had a negligible effect on the values of specific surface area and the crystallite size of La/TiO_2 as compared with TiO_2, N/TiO_2 possessed significantly higher crystallite size and lower specific surface area in contrast to TiO_2. All studied N-La/TiO_2 materials exhibited approximately the same values of both crystallite size and specific surface area that were between those for La/TiO_2 and N/TiO_2. It could be assumed, their value is much more affected by presence of nitrogen (nitrogen doping increases the crystallite size and decreases the specific surface area of N-La/TiO_2 materials).

Table 1 gives the values of the indirect band gap energies of TiO_2, La/TiO_2 and N-La/TiO_2 determined from the dependencies of $(\alpha \cdot h\nu)^{1/2}$ on energy (Fig. 3). The band gap energy of N/TiO_2 was slightly lower (2.93 eV) than for TiO_2. This change could be explained by contribution of both N-doping and the presence of low amount of rutile phase (rutile and anatase have the band gap energy 3.00 and 3.21 eV [49]). The band gap energies of TiO_2, La/TiO_2 and N-La/TiO_2 materials (all containing pure anatase phase) took the values in the range of 2.96–2.99 eV, i.e. the negligible changes of band gap energies were observed after loading of low amount of N and La. Previously, we reported approximately the same band gap energy values for La-TiO_2 photocatalysts with 0.2–1.5 wt% [12], but the absence of a red-shift of absorbance after N-loading is in contrast to other works. In general, addition of N into TiO_2 has been reported to band gap energy narrowing [34,36–38,44,50]. In detail, Valentin et al. [34] reported that states of substitutional nitrogen positions are just above the valence band and the states of interstitial nitrogen positions are higher in the gap. In more detail, 0.77 eV decrease of band gap energy was reported for $La_2Ti_2O_7$ nanosheets after doping of 3.3 at. % of N [37]. However, at lower N-loading (0.07, 0.09 and 0.30 wt% of N in N-TiO_2), Sakthivel et al. [36] measured narrowing of band gap energy of 40–80 meV. The

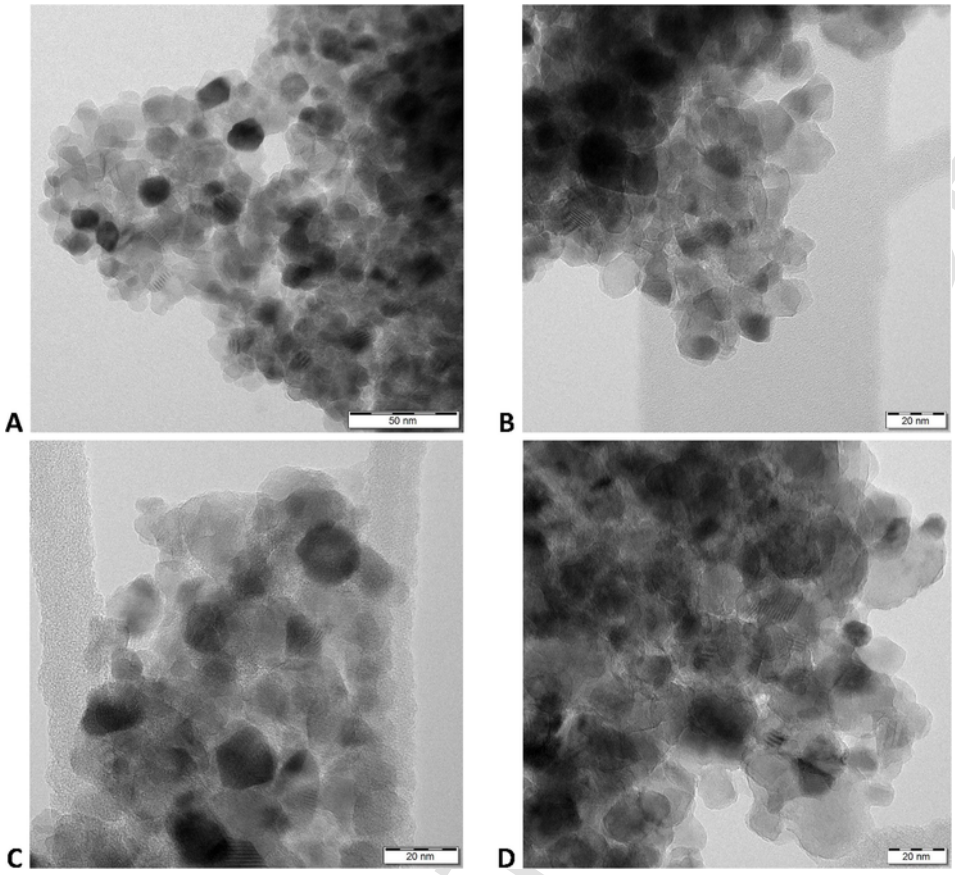

Fig. 2. TEM images of (A) TiO_2, (B) La/TiO_2, (C) 0.97 at. % N-La/TiO_2 and (D) N/TiO_2.

absence of a decrease in band gap energy could be explained by a low nitrogen concentration in our photocatalysts.

Fig. 4a shows the Raman spectra of studied photocatalysts. All spectra showed the bands with a maxima at 144, 195, 396, 515 and 639 cm^{-1}, which are characteristic for the presence of anatase [51]. In contrast to XRD, the presence of rutile was not detected by Raman spectra in N/TiO_2, which can be explained by low content of rutile phase (3 wt% detected by XRD). Fig. 4b shows the detail of the most intensive band with a maximum at 144 cm^{-1} corresponding to E_g phonon mode of anatase. Both the crystallite size (its higher values are leading to red shift to lower wavenumbers) and the amount of oxygen defects (its higher amounts are leading to blue shift to higher wavenumbers) affect the shift of this band [20,22,52]. Both, La/TiO_2 and TiO_2 possess approximately the same position of band and only low difference in the crystallite size, so it is probable that both materials also possess approximately the same amount of oxygen defects. Simultaneously, there was the blue shift observed for N-La/TiO_2 and N/TiO_2 materials in contrast to TiO_2 and La/TiO_2. Whereas a higher crystallinity values for N-La/TiO_2 and N/TiO_2 than for La/TiO_2 and TiO_2 (Table 2) would lead to a red shift, the observed blue shift must be therefore associated with the more pronounced effect of the increased amount of oxygen vacancies presented in N-La/TiO_2 and N/TiO_2 materials than in La/TiO_2 and TiO_2 materials.

XPS analysis identified four different elements (Ti, O, C and N; C and N were observed only in N/ and N-La/TiO_2) presented on the surface of studied photocatalysts. The peak characteristic for the presence of surface La element was not observed, but this is in line with our previous work, where surface La was detected via XPS in La/TiO_2 containing more than 0.80 wt% of La [12]. Two peaks with a binding energy of 458.4 eV and 464.1 eV could be attributed to the binding energy values of Ti $2p_{3/2}$ and $2p_{1/2}$, respectively, both reflecting the presence of Ti^{4+} in TiO_2 lattice. Two different types of oxygen were determined, lattice O^{2-} ions (binding energy of 529.7 eV) and surface hydroxyl groups (binding energy of 530.8 eV). In addition, one peak corresponding to N 1s with a binding energy of 399.7 eV was observed in N-La/TiO_2 and N/TiO_2. This peak could be attributed to the nitrogen in interstitial position [21,33]. On the other hand, absence of peak with a binding energy at 396.9 eV means that nitrogen in substitutional position was not formed in any materials [33]. The dominant presence of nitrogen in interstitial position is in agreement with the work of Powell et al. [38] that reported that the N-TiO_2 materials prepared by using of TMEDA precursor show nitrogen in interstitial position rather than in substitutional position. The amount of C element was 7.1–7.3 at. % in all N-La/TiO_2 photocatalysts and 10.8 at. % in N/TiO_2. It is the residual amount of C after TMEDA precursor.

Table 3 gives the surface concentration of Ti, O and N elements. The values are recalculated without the presence of surface C element. The surface concentration of N element increases from 0.33 to 0.97 at. %. It correlates with the fact that it was below detection limit of AAS that is 0.1 wt% N. It is interesting, that the surface amount of nitrogen is the highest in the materials prepared with the lowest theoretical amount of nitrogen and vice versa. It could be probably explained based on work of Powell et al. [38] that reported the tendency of TMEDA in sol-gel to chelate into a jelly-like polymer. Thus, nitrogen in interstitial position was preferentially formed at lower concentration of TMEDA. The increasing amount of surface N in N-La/TiO_2 photocatalysts was associated with the decreasing amount of total surface oxygen species from 70.47 to 69.26 at. %.

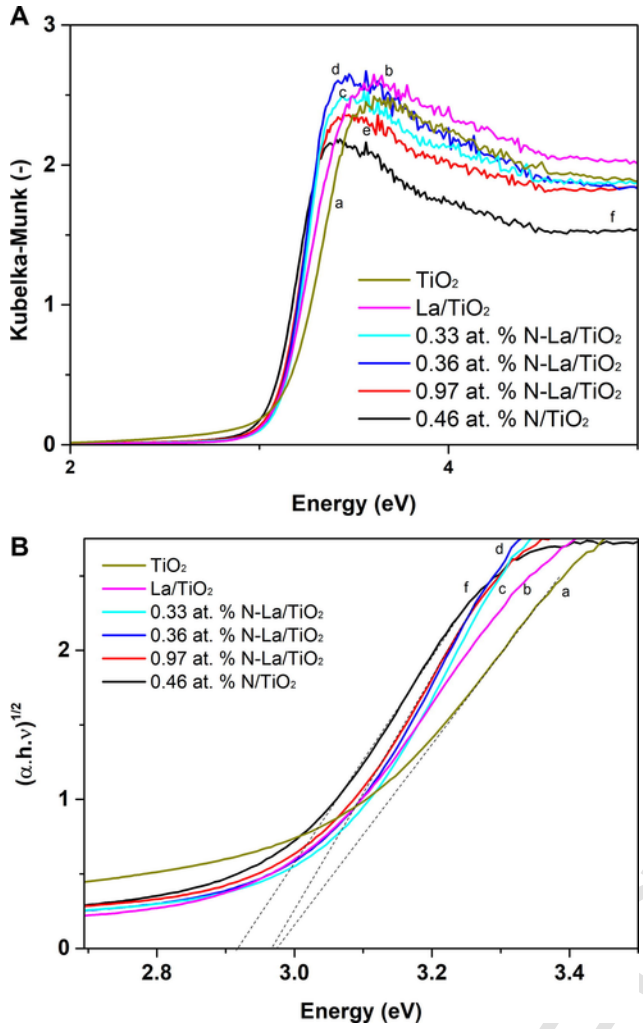

Fig. 3. (A) DR UV/Vis spectra of (a) TiO_2, (b) La/TiO_2, (c) 0.33 at. % N-La/TiO_2, (d) 0.36 at. % N-La/TiO_2, (e) 0.97 at. % N-La/TiO_2, (f) N/TiO_2 recalculated to (B) the dependencies of $(\alpha \cdot h \cdot \nu)^{1/2}$ on energy.

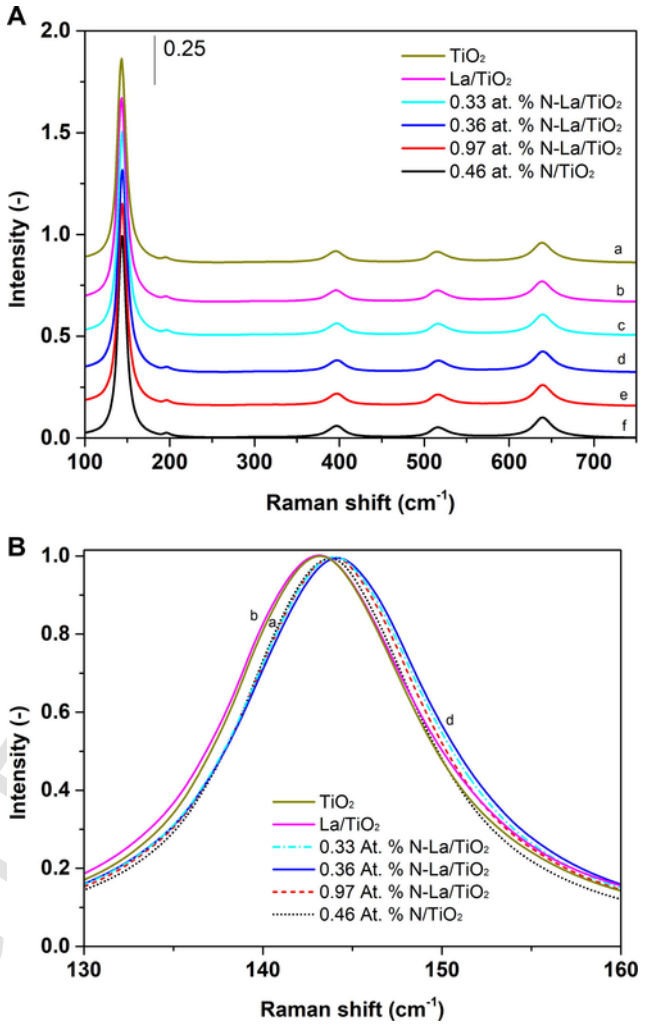

Fig. 4. (A) Raman spectra of (a) TiO_2, (b) La/TiO_2, (c) 0.33 at. % N-La/TiO_2, (d) 0.36 at. % N-La/TiO_2, (e) 0.97 at. % N-La/TiO_2, (f) N/TiO_2 (B) with the detail of the band at 144 cm^{-1}.

3.2. Photocatalytic activity of La/, N/ and N-La/TiO_2

Fig. 5 shows the amount of hydrogen as a function of time. The photocatalytic behaviour tests of all photocatalysts were re-measured two times with the same result. There was observed slight delay in the rise of hydrogen at the beginning of reaction. Negligible amount of hydrogen was formed during photolysis (see our previous work [12]). Fig. 6 compares the amount of hydrogen produced on the individual photocatalysts after 4 h of irradiation. It is evident that pure TiO_2 exhibited the lowest amount of hydrogen. Addition of La to TiO_2 led to an increase in the amount of hydrogen production. We previously studied La/TiO_2 materials containing La between 0.18 and 1.74 wt% of La (based on XRF) with the highest amount of hydrogen produced for 0.18 wt% of La [12]. All N-La/TiO_2 materials produced a significantly higher amount of hydrogen than TiO_2 and La/TiO_2. 0.46 at. % N/TiO_2 exhibited approximately the same photocatalytic behaviour as 0.33 at. % N-La/TiO_2, so the difference in the role of nitrogen content was compensated by the presence of lanthanum. 0.96 at. % N-La/TiO_2 produced highest amount of hydrogen.

It is hard to compare the observed photocatalytic results with a literature, as it is usually measured under different reaction conditions (methanol to water ratio, volume of reaction mixture, amount of catalyst, radiation and time) and sometimes information needed for accurate comparison are missing. High hydrogen yield seems to be published, e.g., for Au- [2,10], Pt- [2,5,6,53] and Cu [3,4,54] based TiO_2 photocatalysts. The close reaction conditions are given, e.g., for Pt/TiO_2-*x*N*x* (150 ml of 1:4 methanol to water solution, 0.65 g of catalyst and 400 W halogen lamp), with reporting hydrogen yield 200 μmol·g^{-1} after 6 h and ca 39 μmol·g^{-1} after 4 h (deduced from the graph) [6]. From that point of view, the observed hydrogen yield of 33 μmol·g^{-1}

Table 3
Surface concentration of Ti, O and N elements based on XPS.

Sample	Ti^{4+} in TiO_2	Lattice O^{2-}, at. %	Hydroxyls OH^-, at. %	Suma O, at. %	N, at. %
TiO_2	29.53	57.66	12.81	70.47	–
La/TiO_2	29.96	61.96	8.08	70.04	–
0.33 at. % N-La/TiO_2	29.74	61.41	8.52	69.92	0.33
0.36 at. % N-La/TiO_2	30.27	59.05	10.32	69.37	0.36
0.97 at. % N-La/TiO_2	29.76	60.88	8.39	69.26	0.97
0.46 at. % N/TiO_2	29.93	57.05	12.57	69.62	0.46

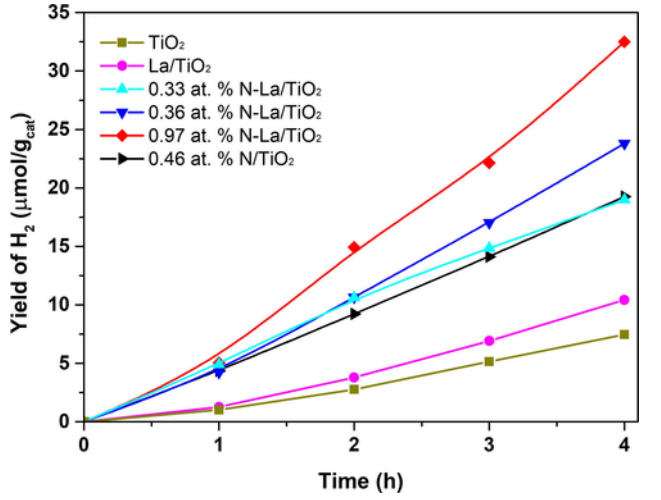

Fig. 5. Dependence of hydrogen yield on time in photocatalytic decomposition of methanol-water solution on N/, La/, N-La/TiO_2 photocatalysts.

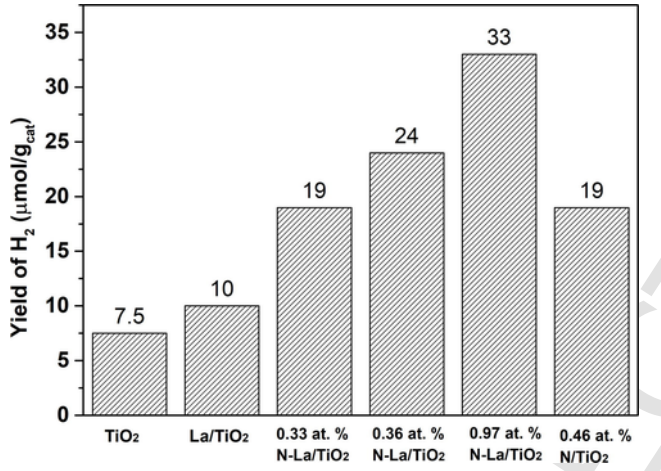

Fig. 6. Comparison of hydrogen yield in photocatalytic decomposition of methanol-water solution N/, La/, N-La/TiO_2 photocatalysts after 4 h.

after 4 h (100 ml of 1:1 methanol to water solution, 1 g of catalyst and 8 W lamp) observed for N-La/TiO_2 (Fig. 5) seems to be interesting.

3.3. The role of nitrogen on the photocatalytic behaviour of N-La/TiO_2

It was shown above that N co-doping in N-La/TiO_2 photocatalysts represents the way, how to increase the amount of hydrogen produced for La/TiO_2 (caption 3.2) which could no longer be improved by loading of La itself [12].

In general, the photocatalytic behaviour could be affected by several factors, such as presence of oxygen vacancies, rate of the recombination of electron-hole pairs, band gap energy, specific surface area and the crystallite size. Extraordinary photocatalytic behaviour of N-La/TiO_2 photocatalysts in many different reactions have been mainly explained by synergistic effect of La and N, i.e. on the basis of the narrowing of the band gap energy, the inhibition of the recombination of electrons and holes and the increase of specific surface area (see Section 1).

In our case, N-La/TiO_2 photocatalysts with a low concentration of surface N (0.33–0.91 surface at. %) and La (0.14–0.16 wt% of La) exhibited lower specific surface area and higher crystallite size than TiO_2 and La/TiO_2. Moreover, N-La/TiO_2 exhibited only negligible decrease in band gap energies in contrast to TiO_2 and La/TiO_2. Increased visible light absorption is one of the reasons for improved photocatalytic behaviour of N-TiO_2 based photocatalyst (e.g. [55]). Despite all these facts, the higher formation of hydrogen was observed in the presence of N-La/TiO_2 than in the presence of La/TiO_2 and TiO_2 photocatalysts.

The absence of a decrease of band gap energy could also be related to the fact that neither the shift of the peak of O1s (not shown in the figure), which reflects the replacement of O^{2-} ions with N^{3-} ions nor the formation of Ti^{3+} ions (XPS results) were observed. Both of these facts are involved in the creation of oxygen vacancies and narrowing the band gap energy [44]. It probably could be explained by low surface concentration of interstitial nitrogen position (XPS) that is however sufficient for improved photocatalytic behaviour of La-N-TiO_2 (Fig. 6).

Formation of nitrogen in interstitial position (XPS) is in agreement with Powell et al. [38] who presented the synthesis of N-La/TiO_2 materials with use of TMEDA precursor. After that, Dunnill et al. [32] reported that even small concentration of interstitial nitrogen promotes the formation of oxygen vacancies. In our case, we assumed, based on Raman spectra, that N-La/TiO_2 photocatalysts possessed higher amount of oxygen vacancies in contrast to TiO_2 and La/TiO_2. This is in agreement with the conclusion of other authors dealing with N-La/TiO_2 photocatalysts [25]. Although, a number of factors influence the photocatalytic behaviour of N-La materials, it can be subsequently assumed that the presence of nitrogen in interstitial position in N-La/TiO_2 plays a significant role in the production of hydrogen over N-La/TiO_2. Unfortunately, the amount of oxygen vacancies is hard to quantify. For example, Valentin et al. [56] reviewed the analysis of oxygen vacancies in N/TiO_2 materials by using the EPR with separation of charged diamagnetic and paramagnetic N-centres. Barbieriková et al. [19] recently correlated the presence of paramagnetic reactive oxygen species with the photocatalytic decomposition of 4-chlorophenol on N/TiO_2.

Fig. 7 shows the dependence of hydrogen amount on the total amount of surface oxygen species in TiO_2, La/TiO_2, N/TiO_2 and N-La/TiO_2 photocatalysts. The increasing yield of hydrogen correlated well with the decreasing surface oxygen content in all materials including TiO_2 and La/TiO_2. Lower amount of surface oxygen in N-La/TiO_2 than in TiO_2 and La/TiO_2 could be explained by doping of low amount of nitrogen in interstitial positions.

4. Conclusion

N-La/TiO_2 materials were prepared with approximately the same amount of La (0.14–0.16 wt%), but changing amount of N

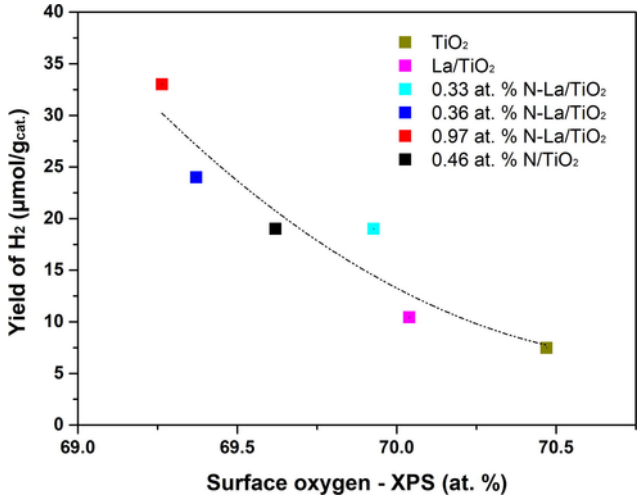

Fig. 7. Dependence of hydrogen yield on the surface oxygen concentration in N/, La/, N-La/TiO_2 photocatalysts.

(0.33–0.97 at. % of surface nitrogen). The hydrogen yield increased in order of TiO_2 < La/TiO_2 < N/TiO_2 (0.46 at. %) < N-La/TiO_2 (0.33 at. %, 0.36 at. % and 0.97 at. % of N). It is evident that the N co-doping led to the improvement of the photocatalytic behaviour of N-La/TiO_2 photocatalysts in contrast to TiO_2 and La/TiO_2. The highest amount of hydrogen was observed for 0.97 at. % N-La/TiO_2 which was 4 times higher in comparison with pure TiO_2. This result demonstrates that co-doping with non-metal and metal ions is more powerful to increase the photoactivity of TiO_2 than doping by single type of ion.

Analysis of chemical composition and structural, textural, surface and optical properties led to the description of several differences in TiO_2, N/TiO_2, La/TiO_2 and N-La/TiO_2 photocatalysts. N/TiO_2 possessed higher crystallite size and lower specific surface area in contrast to TiO_2.

All studied N-La/TiO_2 materials exhibited approximately the same values of both crystallite size and specific surface area that values were between those for La/TiO_2 and N/TiO_2. Negligible changes in band gap energies were observed for N-La/TiO_2 photocatalysts with low concentration of N and La in contrast to TiO_2 and La/TiO_2. The amount of oxygen vacancies (Raman spectroscopy) and the amount of surface oxygen (XPS) were the most evident differences between N-La/TiO_2 photocatalysts on the one hand and TiO_2 and La/TiO_2 photocatalysts on the other. The photocatalytic activity increased with the increasing amount of surface nitrogen and subsequently with increasing amount of oxygen vacancies and decreasing amount of surface oxygen species. Nitrogen and lanthanum co-produce doping could create synergistic effect.

Acknowledgements

Authors thank to the financial support of the Grant Agency of the Czech Republic (project No. 17-20737S). All employees of VŠB-Technical University of Ostrava also thank to the support of the EU structural funding in Operational Programme Research, Development and Education, project No. CZ.02.1.01/0.0/0.0/16_019/0000853 "IET-ER". The XPS measurements (Piotr Kuśtrowski) were carried out with the equipment purchased thanks to the financial support of the European Regional Development Fund in the framework of the Polish Innovation Economy Operational Program (contract no. POIG.02.01.00-12-023/08). Authors thank Dr. I. Troppová for N_2 physisorption, and doc. M. Pouzar for XRF measurements.

References

[1] K.C. Christoforidis, P. Fornasiero, Photocatalytic hydrogen production: a rift into the future energy supply, ChemCatChem 9 (2017) 1523–1544, https://doi.org/10.1002/cctc.201601659.

[2] H. Ahmad, S. Kamarudin, L. Minggu, M. Kassim, Hydrogen from photo-catalytic water splitting process: a review, Renew. Sustain. Energy Rev. 43 (2015) 599–610, https://doi.org/10.1016/j.rser.2014.10.101.

[3] H.-J. Choi, M. Kang, Hydrogen production from methanol/water decomposition in a liquid photosystem using the anatase structure of Cu loaded TiO_2, Int. J. Hydrogen Energy 32 (2007) 3841–3848, https://doi.org/10.1016/j.ijhydene.2007.05.011.

[4] N. Vinothkumar, M. De, Hydrogen production from water–methanol solution over visible light active indium–titanium oxide photocatalysts modified with copper oxide, Int. J. Hydrogen Energy 39 (2014) 11494–11500, https://doi.org/10.1016/j.ijhydene.2014.05.095.

[5] D.W. Hwang, H.G. Kim, J.S. Jang, S.W. Bae, S.M. Ji, J.S. Lee, Photocatalytic decomposition of water–methanol solution over metal-doped layered perovskites under visible light irradiation, Catal. Today 93 (2004) 845–850, https://doi.org/10.1016/j.cattod.2004.06.084.

[6] W.-C. Lin, W.-D. Yang, I.-L. Huang, T.-S. Wu, Z.-J. Chung, Hydrogen production from methanol/water photocatalytic decomposition using Pt/TiO_2−xNx Catalyst, Energy Fuels 23 (2009) 2192–2196, https://doi.org/10.1021/ef801091p.

[7] M.-S. Park, M. Kang, The preparation of the anatase and rutile forms of Ag–TiO_2 and hydrogen production from methanol/water decomposition, Mater. Lett. 62 (2008) 183–187, https://doi.org/10.1016/j.matlet.2007.04.105.

[8] J. Kim, M. Kang, High photocatalytic hydrogen production over the band gap-tuned urchin-like Bi_2S_3-loaded TiO_2 composites system, Int. J. Hydrogen Energy 37 (2012) 8249–8256, https://doi.org/10.1016/j.ijhydene.2012.02.057.

[9] Q. Xie, Y. Wang, B. Pan, H. Wang, W. Su, X. Wang, A novel photocatalyst LaOF: facile fabrication and photocatalytic hydrogen production, Catal. Commun. 27 (2012) 21–25, https://doi.org/10.1016/j.catcom.2012.06.019.

[10] O. Rosseler, M.V. Shankar, M. Karkmaz-Le Du, L. Schmidlin, N. Keller, V. Keller, Solar light photocatalytic hydrogen production from water over Pt and Au/TiO_2 (anatase/rutile) photocatalysts: influence of noble metal and porogen promotion, J. Catal. 269 (2010) 179–190, https://doi.org/10.1016/j.jcat.2009.11.006.

[11] E. Aguiló, L. Soler, A. Casanovas, A.J. Moro, J.C. Lima, L. Rodríguez, J. Llorca, Gold (I)-complex–titania hybrid photocatalyst for hydrogen production, ChemCatChem 9 (2017) 3289–3292, https://doi.org/10.1002/cctc.201700518.

[12] K. Kočí, I. Troppová, M. Edelmannová, J. Starostka, L. Matějová, J. Lang, M. Reli, H. Drobná, A. Rokicińska, P. Kuśtrowski, Photocatalytic decomposition of methanol over La/TiO_2 materials, Environ. Sci. Pollut. Res. (2017) 1–8, https://doi.org/10.1007/s11356-017-0460-x.

[13] Y. Ye, Z. Zang, T. Zhou, F. Dong, S. Lu, X. Tang, W. Wei, Y. Zhang, Theoretical and experimental investigation of highly photocatalytic performance of CuInZnS nanoporous structure for removing the NO gas, J. Catal. 357 (2018) 100–107, https://doi.org/10.1016/j.jcat.2017.11.002.

[14] L. Kong, X. Zhang, C. Wang, F. Wan, L. Li, Synergic effects of Cu_xO electron transfer co-catalyst and valence band edge control over TiO_2 for efficient visible-light photocatalysis, Chin. J. Catal. 38 (2017) 2120–2131, https://doi.org/10.1016/S1872-2067(17)62959-0.

[15] Y. Sohn, W. Huang, F. Taghipour, Recent progress and perspectives in the photocatalytic CO_2 reduction of Ti-oxide-based nanomaterials, Appl. Surf. Sci. 396 (2017) 1696–1711, https://doi.org/10.1016/j.apsusc.2016.11.240.

[16] X. Pan, M.-Q. Yang, X. Fu, N. Zhang, Y.-J. Xu, Defective TiO_2 with oxygen vacancies: synthesis, properties and photocatalytic applications, Nanoscale 5 (2013) 3601–3614, https://doi.org/10.1039/C3NR00476G.

[17] T. Berger, M. Sterrer, O. Diwald, E. Knözinger, Charge trapping and photoadsorption of O_2 on dehydroxylated TiO_2 nanocrystals—an electron paramagnetic resonance study, ChemPhysChem 6 (2005) 2104–2112, https://doi.org/10.1002/cphc.200500161.

[18] J. Nowotny, T. Bak, M.K. Nowotny, L.R. Sheppard, Defect chemistry and electrical properties of titanium dioxide. 1. Defect diagrams, J. Phys. Chem. C 112 (2008) 590–601, https://doi.org/10.1021/jp074565u.

[19] Z. Barbieriková, E. Pližingrová, M. Motlochová, P. Bezdička, J. Boháček, D. Dvoranová, M. Mazúr, J. Kupčík, J. Jirkovský, J. Šubrt, N-doped titanium dioxide nanosheets: preparation, characterization and UV/visible-light activity, Appl. Catal. B 232 (2018) 397–408, https://doi.org/10.1016/j.apcatb.2018.03.053.

[20] S. Sahoo, A. Arora, V. Sridharan, Raman line shapes of optical phonons of different symmetries in anatase TiO_2 nanocrystals, J. Phys. Chem. C 113 (2009) 16927–16933, https://doi.org/10.1021/jp9046193.

[21] A. Fujishima, X. Zhang, D.A. Tryk, TiO_2 photocatalysis and related surface phenomena, Surf. Sci. Rep. 63 (2008) 515–582, https://doi.org/10.1016/j.surfrep.2008.10.001.

[22] M. Meksi, A. Turki, H. Kochkar, L. Bousselmi, C. Guillard, G. Berhault, The role of lanthanum in the enhancement of photocatalytic properties of TiO_2 nanomaterials obtained by calcination of hydrogenotitanate nanotubes, Appl. Catal. B 181 (2016) 651–660, https://doi.org/10.1016/j.apcatb.2015.08.037.

[23] J. Choi, H. Park, M.R. Hoffmann, Effects of single metal-ion doping on the visible-light photoreactivity of TiO_2, J. Phys. Chem. C 114 (2009) 783–792, https://doi.org/10.1021/jp908088x.

[24] R.D. Shannon, Revised effective ionic radii and systematic studies of interatomic distances in halides and chalcogenides, Acta Crystallogr. Sect. A: Cryst. Phys. Diffract. Theor. Gen. Crystallogr. 32 (1976) 751–767, https://doi.org/10.1107/S0567739476001551.

[25] J. Zhang, Z. Zhao, X. Wang, T. Yu, J. Guan, Z. Yu, Z. Li, Z. Zou, Increasing the oxygen vacancy density on the TiO_2 surface by La-doping for dye-sensitized solar cells, J. Phys. Chem. C 114 (2010) 18396–18400, https://doi.org/10.1021/jp106648c.

[26] J. Liqiang, S. Xiaojun, X. Baifu, W. Baiqi, C. Weimin, F. Honggang, The preparation and characterization of La doped TiO_2 nanoparticles and their photocatalytic activity, J. Solid State Chem. 177 (2004) 3375–3382, https://doi.org/10.1016/j.jssc.2004.05.064.

[27] A.-W. Xu, Y. Gao, H.-Q. Liu, The preparation, characterization, and their photocatalytic activities of rare-earth-doped TiO_2 nanoparticles, J. Catal. 207 (2002) 151–157, https://doi.org/10.1006/jcat.2002.3539.

[28] Z.-L. Ma, G.-F. Huang, D.-S. Xu, M.-G. Xia, W.-Q. Huang, Y. Tian, Coupling effect of La doping and porphyrin sensitization on photocatalytic activity of nanocrystalline TiO_2, Mater. Lett. 108 (2013) 37–40, https://doi.org/10.1016/j.matlet.2013.06.080.

[29] Q. Wang, S. Xu, F. Shen, Preparation and characterization of TiO_2 photocatalysts co-doped with iron (III) and lanthanum for the degradation of organic pollutants, Appl. Surf. Sci. 257 (2011) 7671–7677, https://doi.org/10.1016/j.apsusc.2011.03.157.

[30] S.G. Kumar, K.K. Rao, Comparison of modification strategies towards enhanced charge carrier separation and photocatalytic degradation activity of metal oxide semiconductors (TiO_2, WO_3 and ZnO), Appl. Surf. Sci. 391 (2017) 124–148, https://doi.org/10.1016/j.apsusc.2016.07.081.

[31] Y. Cong, B. Tian, J. Zhang, Improving the thermal stability and photocatalytic activity of nanosized titanium dioxide via La^{3+} and N co-doping, Appl. Catal. B 101 (2011) 376–381, https://doi.org/10.1016/j.apcatb.2010.10.006.

[32] C.W. Dunnill, I.P. Parkin, Nitrogen-doped TiO_2 thin films: photocatalytic applications for healthcare environments, Dalton Trans. 40 (2011) 1635–1640, https://doi.org/10.1039/C0DT00494D.
[33] R. Asahi, T. Morikawa, T. Ohwaki, K. Aoki, Y. Taga, Visible-light photocatalysis in nitrogen-doped titanium oxides, Science 293 (2001) 269–271, https://doi.org/10.1126/science.1061051.
[34] C. Di Valentin, G. Pacchioni, A. Selloni, S. Livraghi, E. Giamello, Characterization of paramagnetic species in N-doped TiO_2 powders by EPR spectroscopy and DFT calculations, J. Phys. Chem. B 109 (2005) 11414–11419, https://doi.org/10.1021/jp051756t.
[35] P. Zhang, Y. Yu, E. Wang, J. Wang, J. Yao, Y. Cao, Structure of nitrogen and zirconium co-doped titania with enhanced visible-light photocatalytic activity, ACS Appl. Mater. Interfaces 6 (2014) 4622–4629, https://doi.org/10.1021/am405510a.
[36] S. Sakthivel, M. Janczarek, H. Kisch, Visible light activity and photoelectrochemical properties of nitrogen-doped TiO_2, J. Phys. Chem. B 108 (2004) 19384–19387, https://doi.org/10.1021/jp046857q.
[37] F. Meng, Z. Hong, J. Arndt, M. Li, M. Zhi, F. Yang, N. Wu, Visible light photocatalytic activity of nitrogen-doped $La_2Ti_2O_7$ nanosheets originating from band gap narrowing, Nano Res. 5 (2012) 213–221, https://doi.org/10.1007/s12274-012-0201-x.
[38] M.J. Powell, C.W. Dunnill, I.P. Parkin, N-doped TiO_2 visible light photocatalyst films via a sol–gel route using TMEDA as the nitrogen source, J. Photochem. Photobiol., A 281 (2014) 27–34, https://doi.org/10.1016/j.jphotochem.2014.03.003.
[39] Y. Yu, L. Piao, J. Xia, W. Wang, J. Geng, H. Chen, X. Xing, H. Li, A facile one-pot synthesis of N-La codoped TiO_2 porous materials with bio-hierarchical architectures and enhanced photocatalytic activity, Mater. Chem. Phys. 182 (2016) 77–85, https://doi.org/10.1016/j.matchemphys.2016.07.007.
[40] D. Liu, Z. Wu, F. Tian, B.-C. Ye, Y. Tong, Synthesis of N and La co-doped TiO_2/AC photocatalyst by microwave irradiation for the photocatalytic degradation of naphthalene, J. Alloy. Compd. 676 (2016) 489–498, https://doi.org/10.1016/j.jallcom.2016.03.124.
[41] Y. Chen, Q. Wu, C. Zhou, Q. Jin, Enhanced photocatalytic activity of La and N co-doped TiO_2/diatomite composite, Powder Technol. 322 (2017) 296–300, https://doi.org/10.1016/j.powtec.2017.09.026.
[42] L. Yu, X. Yang, J. He, Y. He, D. Wang, One-step hydrothermal method to prepare nitrogen and lanthanum co-doped TiO_2 nanocrystals with exposed 0 0 1 facets and study on their photocatalytic activities in visible light, J. Alloys Compd. 637 (2015) 308–314, https://doi.org/10.1016/j.jallcom.2015.03.035.
[43] J. Liu, H. Li, L. Zong, Q. Li, X. Wang, M. Zhang, J. Yang, Photocatalytic oxidation of propylene on La and N codoped TiO_2 nanoparticles, J. Nanopart. Res. 17 (2015) 114, https://doi.org/10.1007/s11051-015-2916-6.
[44] T. Jia, F. Fu, D. Yu, J. Cao, G. Sun, Facile synthesis and characterization of N-doped TiO_2/C nanocomposites with enhanced visible-light photocatalytic performance, Appl. Surf. Sci. 430 (2018) 438–447, https://doi.org/10.1016/j.apsusc.2017.07.024.
[45] Y. Li, S. Cao, A. Zhang, C. Zhang, T. Qu, Y. Zhao, A. Chen, Carbon and nitrogen co-doped bowl-like Au/TiO_2 nanostructures with tunable size for enhanced visible-light-driven photocatalysis, Appl. Surf. Sci. 445 (2018) 350–358, https://doi.org/10.1016/j.apsusc.2018.03.187.
[46] M.S. Akple, J. Low, S. Liu, B. Cheng, J. Yu, W. Ho, Fabrication and enhanced CO_2 reduction performance of N-self-doped TiO_2 microsheet photocatalyst by bi-cocatalyst modification, J. CO_2 Util. 16 (2016) 442–449, https://doi.org/10.1016/j.jcou.2016.10.009.
[47] K. Kočí, I. Troppová, M. Reli, L. Matějová, M. Edelmannová, H. Drobná, L. Dubnová, A. Rokicińska, P. Kuśtrowski, L. Čapek, Nd/TiO_2 anatase-brookite photocatalysts for photocatalytic decomposition of methanol, Front. Chem. 6 (2018) 44, https://doi.org/10.3389/fchem.2018.00044.
[48] A.T. Dal'Toé, G.L. Colpani, N. Padoin, M.A. Fiori, C. Soares, Lanthanum doped titania decorated with silver plasmonic nanoparticles with enhanced photocatalytic activity under UV-visible light, Appl. Surf. Sci. 441 (2018) 1057–1071, https://doi.org/10.1016/j.apsusc.2018.01.291.
[49] D. Reyes-Coronado, G. Rodríguez-Gattorno, M. Espinosa-Pesqueira, C. Cab, R.d. de Coss, G. Oskam, Phase-pure TiO_2 nanoparticles: anatase, brookite and rutile, Nanotechnology 19 (2008) 145605, https://doi.org/10.1088/0957-4484/19/14/145605.
[50] J. Low, B. Cheng, J. Yu, Surface modification and enhanced photocatalytic CO_2 reduction performance of TiO_2: a review, Appl. Surf. Sci. 392 (2017) 658–686, https://doi.org/10.1016/j.apsusc.2016.09.093.
[51] U. Balachandran, N. Eror, Raman spectra of titanium dioxide, J. Solid State Chem. 42 (1982) 276–282, https://doi.org/10.1016/0022-4596(82)90006-8.
[52] Y. Huo, J. Zhu, J. Li, G. Li, H. Li, An active La/TiO_2 photocatalyst prepared by ultrasonication-assisted sol–gel method followed by treatment under supercritical conditions, J. Mol. Catal. A: Chem. 278 (2007) 237–243, https://doi.org/10.1016/j.molcata.2007.07.054.
[53] A. Meng, J. Zhang, D. Xu, B. Cheng, J. Yu, Enhanced photocatalytic H_2-production activity of anatase TiO_2 nanosheet by selectively depositing dual-cocatalysts on 101 and 001 facets, Appl. Catal. B 198 (2016) 286–294, https://doi.org/10.1016/j.apcatb.2016.05.074.
[54] W. Chen, Y. Wang, S. Liu, L. Gao, L. Mao, Z. Fan, W. Shangguan, Z. Jiang, Non-noble metal Cu as a cocatalyst on TiO_2 nanorod for highly efficient photocatalytic hydrogen production, Appl. Surf. Sci. 445 (2018) 527–534, https://doi.org/10.1016/j.apsusc.2018.03.209.
[55] M.S. Akple, J. Low, Z. Qin, S. Wageh, A.A. Al-Ghamdi, J. Yu, S. Liu, Nitrogen-doped TiO_2 microsheets with enhanced visible light photocatalytic activity for CO_2 reduction, Chin. J. Catal. 36 (2015) 2127–2134, https://doi.org/10.1016/S1872-2067(15)60989-5.
[56] C. Di Valentin, E. Finazzi, G. Pacchioni, A. Selloni, S. Livraghi, M.C. Paganini, E. Giamello, N-doped TiO_2: theory and experiment, Chem. Phys. 339 (2007) 44–56, https://doi.org/10.1016/j.chemphys.2007.07.020.